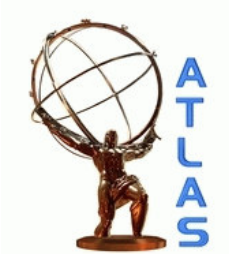

ATLAS NOTE

ATLAS-CONF-2010-066

July 20, 2010

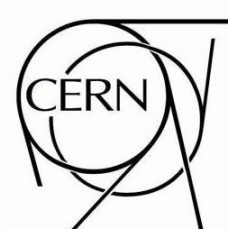

Early supersymmetry searches with jets, missing transverse momentum and one or more leptons with the ATLAS Detector

ATLAS collaboration

Abstract

This note describes a first set of measurements of supersymmetry-sensitive variables in the final states with jets, missing transverse momentum and leptons using the $\sqrt{s} = 7$ TeV proton-proton collisions at the LHC. The data were collected during the period March 2010 to July 2010 and correspond to a total integrated luminosity of $70 \pm 8\,\text{nb}^{-1}$. Agreement is found between data and Monte Carlo simulations indicating that the Standard Model backgrounds to searches for new physics are under control.

1 Introduction

Supersymmetry (SUSY) [1] is a theoretically favoured candidate for physics beyond the Standard Model. If strongly interacting supersymmetric particles are present at the TeV-scale, then such particles should be copiously produced in the 7 TeV collisions at the Large Hadron Collider [2]. The ATLAS [3] collaboration has already reported the observation of the electroweak $W^{\pm}$ and Z^0 bosons [4], and of high transverse-momentum jets [5]. With increasing integrated luminosities the LHC experiments will achieve sensitivity to the production of supersymmetric particles [6] exceeding that of the Tevatron experiments [7].

This note presents a first comparison of data to Monte Carlo simulations for some of the most important kinematical variables that are expected to be employed in supersymmetry searches involving jets and missing transverse momentum and one or more isolated leptons (electrons or muons). Selections based on these variables are expected to be sensitive not only to *R*-parity conserving SUSY particle production, but also to any model in which one or more strongly-interacting particles decay semi-invisibly producing leptons and jets.

2 The ATLAS detector

The ATLAS detector is described in detail elsewhere [3]. The analysis presented makes use of almost all detector components.

The ATLAS inner tracking detector is immersed in a 2 T magnetic field provided by a superconducting solenoid. Charged particle position measurements are made by silicon pixel and microstrip detectors in the pseudorapidity[1)] range $|\eta| < 2.5$ and by a straw tube tracker in the range $|\eta| < 2.0$ which enhances electron identification by the detection of transition-radiation photons.

The calorimeters instrument the range $|\eta| < 4.9$, using a variety of detector technologies. The lead-liquid argon (LAr) electromagnetic calorimeter is divided into a barrel part ($|\eta| < 1.475$) and the two endcap components ($1.375 < |\eta| < 3.2$). The hadronic tile calorimeter is placed directly outside the barrel electromagnetic calorimeter envelope. This steel/scintillating-tile detector consists of a barrel covering the region $|\eta| < 1.0$ and two extended barrels in the range $0.8 < |\eta| < 1.7$. The copper-LAr hadronic endcap calorimeter consists of two independent wheels per endcap ($1.5 < |\eta| < 3.2$) located directly behind the endcap electromagnetic calorimeter. Larger values of $|\eta|$ (up to $|\eta| < 4.9$) are covered by the forward calorimeters which consist of three modules in each endcap: the first made of copper-LAr is optimized for electromagnetic measurements while the other two made of tungsten-LAr measure primarily the energy of hadronic interactions.

The muon spectrometer measures the deflection of muon tracks in the field of three large superconducting air-core toroid magnets. It is instrumented with separate trigger and high-precision tracking chambers. The trigger is provided by resistive plate chambers in the barrel ($|\eta| < 1.05$) and thin gap chambers in the endcap regions (up to $|\eta| = 2.4$). Over most of the pseudorapidity range precision measurements in the principle bending direction are made with monitored drift tubes. The range $2 < |\eta| < 2.7$ of the innermost of the three layers is covered by higher granularity cathode strip chambers.

[1)] The coordinate system employed has its origin at the nominal interaction point. The beam direction defines the *z*-axis and the $x-y$ plane is transverse to the beam direction. The positive *x*-axis is defined as pointing from the interaction point to the centre of the LHC ring and the positive *y*-axis is defined as pointing upwards. The azimuthal angle ϕ is measured around the beam axis and the polar angle θ is the angle from the beam axis. The pseudorapidity is defined as $\eta = -\ln\tan(\theta/2)$. The transverse momentum p_{T}, the transverse energy E_{T}, and the transverse missing energy $E_{\mathrm{T}}^{\mathrm{miss}}$ are defined in the $x-y$ plane. The distance ΔR in the η, ϕ space is defined as $\Delta R = \sqrt{\Delta\eta^2 + \Delta\phi^2}$.

Physics process	Cross section × BR / nb	Luminosity / nb^{-1}
Di-jets (QCD) $8 \leq \hat{p}_{\mathrm{T}} < 17$ GeV	9.85×10^6	0.14
Di-jets (QCD) $17 \leq \hat{p}_{\mathrm{T}} < 35$ GeV	6.78×10^5	2.06
Di-jets (QCD) $35 \leq \hat{p}_{\mathrm{T}} < 70$ GeV	4.10×10^4	34.1
Di-jets (QCD) $70 \leq \hat{p}_{\mathrm{T}} < 140$ GeV	2.20×10^3	636
Di-jets (QCD) $140 \leq \hat{p}_{\mathrm{T}} < 280$ GeV	88	1.59×10^4
Di-jets (QCD) $280 \leq \hat{p}_{\mathrm{T}} < 560$ GeV	2.35	5.96×10^5
Di-jets (QCD) 560 GeV $\leq \hat{p}_{\mathrm{T}}$	0.034	4.12×10^7
$W \to e\nu$	10.45	2.0×10^5
$W \to \mu\nu$	10.45	2.0×10^5
$W \to \tau\nu$	10.45	2.0×10^5
$Z \to \nu\bar{\nu}$	5.82	1.0×10^5
$Z \to e^+e^-$	0.79	5.0×10^5
$Z \to \mu^+\mu^-$	0.79	5.0×10^5
$Z \to \tau^+\tau^-$	0.79	5.0×10^5
$t\bar{t}$	0.164	7.0×10^6
SU4 SUSY point	0.060	11.9×10^5

Table 1: Standard model and SUSY benchmark point Monte Carlo samples used in this analysis including cross section times branching ratio and the equivalent integrated luminosity of the sample. $\hat{p}_{\mathrm{T}}$ is the transverse momentum of the two partons involved in the hard scattering process. The cross sections reported are given at NNLO for $W \to l\nu$ and $Z \to \nu\bar{\nu}$, at NLO with NLL for $t\bar{t}$ and at leading order for jet production via QCD processes (referred to as QCD in the following) and $Z \to l^+l^-$.

3 Monte Carlo simulation

The results presented are compared to expectations based on Monte Carlo simulations. The signal and background samples used were generated at $\sqrt{s} = 7$ TeV. Samples generated with `PYTHIA` [8] and `HERWIG` [9] (with `JIMMY` [10]) used a set of parameters tuned by ATLAS for its 2009 Monte Carlo generation [11]. All signals and backgrounds were passed through a `GEANT4` [12] based simulation and were reconstructed with the same algorithms used for the data. The samples used are summarized in Table 1.

QCD jet production A large sample of inclusive jet events has been generated with `PYTHIA` 6.4.21. The hard interaction of the event is modelled via $2 \to 2$ leading order matrix elements. Additional initial and final state radiations are generated by a parton shower algorithm in the leading logarithm approximation. Multiple interactions are simulated by extra $2 \to 2$ processes according to the ATLAS tunes [11]. Parton density functions are based on MRST 2007 LO* [13]. Given the uncertainties on the rate of such events, the QCD jet production is normalized to data in dijet control regions as described in Section 7.

For the single-muon channel the QCD samples of Table 1 were compared against other samples: sample (b) similar to the QCD sample in Table 1 but with a filter applied requiring a muon with $p_{\mathrm{T}} > 10$ GeV and $|\eta| < 2.8$ in the event record before detector simulation; and sample (c) similar to the `PYTHIA` sample but producing only $b\bar{b}$ at the parton level and so having a larger integrated luminosity than that in Table 1. All of which gave consistent expectations within the statistical uncertainties of the samples. For

the single-muon channel only, the muon-filtered sample (b) which corresponds to the largest integrated luminosity generated for that channel has been used in what follows.

A cross-check of the QCD background has also been performed by comparing the PYTHIA QCD prediction with a set of ALPGEN QCD samples sliced in the p_{T} and the number of partons in the hard scattering process. For the kinematic region that it has been possible to explore, and with the existing experimental uncertainties, there are no material differences between the predictions given by two generators.

Electroweak boson + jets production The production of $W^{\pm}$ or Z^0 bosons in association with jets is expected to be one of the most important backgrounds for supersymmetry searches both with and without leptons. As the SUSY event selection often requires many jets in the final state, it is important to model multiparton final states. For this reason, the ALPGEN [14] Monte Carlo generator which includes electroweak and QCD effects for multiparton hard processes has been chosen. Jet production was generated for up to five-parton matrix elements, in different slices of momentum of the hard process ($\hat{p}_{\mathrm{T}}$). The generator is interfaced to HERWIG [9] for showering and fragmentation processes and to JIMMY [10] for underlying event simulation. The parton density function set used for these samples was CTEQ6L1 [15]. The samples were initially normalized to the integrated luminosity accumulated using the cross sections shown in Table 1 based on next-to-next-to-leading order (NNLO) QCD calculations from the FEWZ program [16]. For the one-lepton channels a refined normalization of the $W^{\pm} \to l\nu$+jets background has been determined by measuring the number of events in a $W^{\pm}$ + two-jet control region as described in Section 7. In each case the same normalization factors have been applied for all ALPGEN matrix element parton multiplicities.

The Drell-Yan production of events with two leptons is generated with PYTHIA. A cut on the invariant mass of the intermediate vector boson has been applied to separate this low $m_{\ell\ell}$ sample from the Z^0 production samples described above.

Top pair production The $t\bar{t}$ process is an important background for most of the SUSY channels described. The MC@NLO [17, 18] generator, including full next-to-leading order QCD corrections has been used to simulate the hard process. Parton showering and fragmentation were simulated by the HERWIG event generator with JIMMY [10] generating the underlying event. The $t\bar{t}$ cross sections were normalized to the next-to-leading order result including next-to-leading log resummation corrections [19]. The CTEQ6.6 next-to-leading-order parton set is used for the matrix element, the parton shower and the underlying event.

Supersymmetry model Kinematic distributions are compared for illustrative purposes to the prediction from a supersymmetric mSUGRA [20] benchmark point. The point chosen SU4 is a low mass point close to the Tevatron limits [7] with $m_0 = 200\,\mathrm{GeV}$, $m_{1/2} = 160\,\mathrm{GeV}$, $A_0 = -400\,\mathrm{GeV}$, $\tan\beta = 10$ and $\mu > 0$. The SU4 mass spectrum and branching ratios were calculated using ISAJET [21] version 7.75. A sample of 5×10^4 inclusive supersymmetry production events were generated with the HERWIG++ generator [22] version 2.4.2 using the MRST 2007 LO* parton density distributions [13]. The inclusive SUSY production cross section is calculated at leading order by HERWIG++ to be 42.3 pb and by Prospino [23] at next-to-leading order to be 59.9 pb. For this model point the typical masses of the strongly interacting particles are in the range 410 to 420 GeV. In the figures presented the SU4 sample is normalized to ten times the next-to-leading-order (Prospino) cross section, for illustrative purposes.

4 Data and Trigger Selection

The measurements presented are based on the $\sqrt{s} = 7$ TeV proton-proton collisions from the LHC and were recorded between March and July 2010. They correspond to a total integrated luminosity of approximately $70 \pm 8\,\text{nb}^{-1}$.

The single muon and dimuon analyses use the events recorded by the ATLAS L1 hardware-based trigger `L1_MU6` which selects events with a hit pattern in the muon chambers consistent with a track with transverse momentum larger than about 6 GeV. The trigger efficiency has been measured for events containing one muon with $p_{\text{T}} > 20$ GeV (using the muon definition described in Section 5.1) from independently triggered events. It is measured to be $(73 \pm 5)\%$ in the region $|\eta| < 1.05$ and $(82 \pm 4)\%$ in the region $1.05 < |\eta| < 2.4$. The corresponding efficiencies in the Monte Carlo are $(80 \pm 3)\%$ in the region $|\eta| < 1.05$ and $(93 \pm 3)\%$ in the region $1.05 < |\eta| < 2.4$. The efficiency becomes constant within statistical uncertainties for muons with p_{T} above 8 GeV, well below the threshold for selecting muons in the analyses.

The single electron, dielectron and electron-muon analyses use events selected first by the L1 hardware-based calorimeter trigger `L1_EM5`, selecting events on the basis of the energy deposited in the electromagnetic calorimeter and calorimeter information with reduced granularity. To further reduce the rate, events passing the first level trigger are further required to pass the `EF_g10_Loose` high level trigger which examines the region of interest flagged by the first level trigger, and selects electromagnetic calorimeter deposits with transverse energies $> 10\,\text{GeV}$. The combined efficiency of this electron trigger chain has been measured for events containing one electron with $p_{\text{T}} > 20$ GeV (using the electron definition described in Section 5.1) from independently-triggered events. The efficiency becomes constant within uncertainties for electrons with $p_{\text{T}} > 15$ GeV and equal to be $(100^{+0}_{-10})\%$. The corresponding efficiency is computed in the Monte Carlo simulation and found to be $(96 \pm 3)\%$.

5 Lepton, jet and missing transverse momentum reconstruction

A general search strategy for *R*-parity conserving SUSY signatures would be the selection of events with large missing transverse momentum and reconstructed particles with large transverse momentum. At the LHC these objects are predominantly jets since the coupling strength of the strong force would cause an abundance of squarks and gluinos if these particles are not prohibitively heavy. Squarks or gluinos will cascade decay to final states containing jets, possibly leptons or photons, depending on the SUSY parameters, and missing transverse momentum caused by any neutrinos and/or stable invisible SUSY particles. The same object identification criteria are used for all channels.

5.1 Object selection

The following criteria are used to select different particle candidates that are used in the event selection. These selection criteria are similar to the ones used in Ref. [24].

Jets are reconstructed with the anti-k_t algorithm [25] which is an infrared safe and collinear safe jet clustering algorithm. The parameter which sets the maximum distance from the jet core to any constituent cluster is $R = 0.4$. The jet algorithm is run on topological clusters which reconstruct a three-dimensional shower topology. The jets are then required to satisfy $p_{\text{T}}^{\text{jet}} > 20$ GeV and $|\eta| < 2.5$, where $p_{\text{T}}^{\text{jet}}$ is the transverse momentum at the hadronic scale.

A set of cleaning cuts is applied to reject events containing jets which are consistent with calorimeter noise, cosmic rays or out-of-time energy deposits. Algorithms for identifying problematic jets are documented elsewhere [26] and have been further refined for early SUSY searches [27].

Any jets passing this loose selection are considered when applying the object identification described in Section 5.2. Larger transverse momenta are required for jets to enter the final selections described in Section 6.

Electrons are reconstructed by algorithms that provide a good separation between isolated electrons and a fake signature from hadronic jets. This paper uses the medium level selection criteria based on shower shape variables combined with track information. In addition to those standard cuts, the p_{T} of electrons is required to be larger then 10 GeV and $|\eta| < 2.47$. Here η of the electrons is considered as the η of the second sampling layer of the electromagnetic calorimeter. Electrons that have $1.37 < |\eta| < 1.52$ are rejected from the selection. This particular region of η has the transition between barrel and endcap calorimeter thus provides unreliable electron identification. To obtain a more isolated electron candidate, the calorimeter energy around the electron is required to be less than 10 GeV within a cone of radius $\Delta R = 0.2$.

Muon candidates are reconstructed by algorithms which perform a statistical combination of a track reconstructed in the muon spectrometer with its corresponding track in the inner detector. The p_{T} of the muons is required to be larger than 10 GeV. The pseudorapidity of muons must satisfy $|\eta| < 2.4$. Muons are required to have a match-χ^2 to be smaller than 100, where match-χ^2 is defined as the difference between outer and inner track vectors weighted by their combined covariance matrix. An isolated muon is obtained by requiring calorimeter energy around the muon to be less than 10 GeV within a cone of $\Delta R = 0.2$.

Missing transverse momentum is formed from two components. The first component is obtained from the vector sum of the transverse energies of all three-dimensional topological clusters in the calorimeter. The second component is obtained from the vector sum of the transverse momenta of the selected well-isolated muons in the analysis[2)]. The total missing transverse momentum is computed by a vector sum of these two components.

5.2 Resolving overlapping objects

When candidates passing the object selection overlap with each other, a classification is required to remove all but one of the overlapping objects. All overlapping criteria are based on the simple geometric $\Delta R = \sqrt{\Delta\phi^2 + \Delta\eta^2}$ variable and applied in the following order based on previous studies [24] :

1. If an electron and a jet are found within $\Delta R < 0.2$, the object is interpreted as an electron and the overlapping 'jet' is ignored.

2. If a muon and a jet are found within $\Delta R < 0.4$, the object is treated as a jet and the muon is rejected.

3. If an electron and a jet are found within $0.2 \leq \Delta R < 0.4$, the object is interpreted as jet and the nearby 'electron' is ignored.

6 Event selection

The results presented were collected from March to July 2010. From all data taken at a centre-of-mass energy of 7 TeV and for which the LHC declared stable beams, only those with the detector high voltage in optimal condition are selected. In addition both the solenoid and toroid must be on at nominal conditions to allow good momentum measurements for the electrons and muons. It is also required

[2)] Contributions from non-isolated and poorly reconstructed muons are not included in the calculation in either the data or the Monte Carlo samples since otherwise poorly reconstructed muons would dominate in the tail of the distribution.

	Data	Monte Carlo	Normalization factor
Electron channel	101	245	0.41 ± 0.08
Muon channel	15	31.4	0.48 ± 0.12

Table 2: The numbers of events in data and the Monte Carlo expectations are shown in the control region used to normalise the QCD dijet background. The control region is defined by $m_{\mathrm{T}} < 40$ GeV and $E_{\mathrm{T}}^{\mathrm{miss}} < 40$ GeV.

that the status of the sub-detectors be sufficiently good that electron, muon, and jet identification as well as energy and momentum computations do not deviate significantly from their expected behaviour. This includes the systems needed for missing transverse momentum reconstruction, as well as the single lepton trigger systems. These basic data-quality requirements resulted in a total integrated luminosity of $70 \pm 8\,\mathrm{nb}^{-1}$ (the same such requirements are used for the electron and muon modes).

In all channels, events are vetoed if an electron passes the object selection in the electromagnetic calorimeter transition region $1.37 < |\eta| < 1.52$. The cut is applied to exclude electrons reconstructed in the barrel-endcap transition region of the electromagnetic calorimeter that will not be properly calibrated with early data. We also veto events with a calorimeter problem in the region covered by the cluster associated to an electron object.

In addition to the electron crack veto described in Section 5.1, the pre-selection cuts are as follows.

1. Require that events have at least one well-reconstructed lepton (electron or muon) with $p_{\mathrm{T}} > 10$ GeV. [3)]

2. Reject events which contain a bad jet as described in Section 5.1. The fraction of triggered events removed by this requirement is about 2×10^{-4} in both the muon and the electron triggered samples.

3. Reject events which do not contain a primary vertex with at least five associated tracks. This cut removes about 3×10^{-3} of the remaining events in the electron-triggered channel and about 15% of the remaining events in the muon-triggered channel. A larger proportion of the events fail this cut in the early data runs when the instantaneous luminosity was relatively smaller suggesting that a significant proportion of the events rejected are unrelated to the proton-proton collisions.

Further selections are applied for both the one lepton channels and for the dilepton channels.

- One lepton channels: there must be exactly one lepton with $p_{\mathrm{T}} > 10$ GeV and that lepton must have $p_{\mathrm{T}} > 20$ GeV. Two or more good jets with pseudorapidity $|\eta| < 2.5$ and jet transverse momentum $p_{\mathrm{T}} > 30$ GeV are required.

- Dilepton channels: there should be two or more leptons with $p_{\mathrm{T}} > 10$ GeV, at least one of which must have $p_{\mathrm{T}} > 20$ GeV. The dilepton invariant mass must be larger than 5 GeV.

7 Control regions and sample normalization

Normalization of the PYTHIA QCD expectation The PYTHIA QCD Monte Carlo is only leading order in the strong coupling constant and thus is not expected to correctly describe the absolute normalization of the dijet cross section.

A control region is defined to rescale the absolute normalization of PYTHIA to the data. The selection criteria for the control region are a cut on the transverse mass $m_{\mathrm{T}} < 40$ GeV and the requirement of

[3)] A separate analysis for events without leptons can be found elsewhere [27].

Channel	Observed	W expectation	Other SM expectation
Electron	6	2.2	0.8
Muon	4	2.1	0.3

Table 3: Number of observed and expected events in the $W^{\pm}$ + jets control region.

missing transverse momentum $E_{\mathrm{T}}^{\mathrm{miss}} < 40$ GeV where the transverse mass of the lepton and the $E_{\mathrm{T}}^{\mathrm{miss}}$ two-vector is defined by

$$m_{\mathrm{T}}^2 \equiv 2|\mathbf{p}_{\mathrm{T}}^{\ell}||E_{\mathrm{T}}^{\mathrm{miss}}| - 2\mathbf{p}_{\mathrm{T}}^{\ell} \cdot \vec{E}_{\mathrm{T}}^{\mathrm{miss}}.$$

This region is expected from simulation to be dominated by QCD dijet production. The normalization factors are shown in Table 2. To allow for any differences between data and Monte Carlo in the rate at which QCD events lead to reconstructed electrons or muons, the normalization factor is derived separately for each lepton species.

Events in the dilepton channel are normalized to the QCD cross section. The normalization was verified in a control region defined by $5 < m_{ll} < 15$ GeV and $E_{\mathrm{T}}^{\mathrm{miss}} < 15$ GeV where the QCD background is expected to dominate. We have assigned a total systematic uncertainty of 100% to the QCD background in the dilepton channel.

Normalization of the `ALPGEN` $W^{\pm}$ + jets expectation For higher jet multiplicities the normalization of the $W^{\pm}$ + jets prediction can suffer from higher order corrections which have been found to be significant at the Tevatron [28].

The normalization of the $W^{\pm}$ +jet prediction for ≥ 2 jets has therefore been determined in a separate control region in which 30 GeV $< E_{\mathrm{T}}^{\mathrm{miss}} <$ 50 GeV and 40 GeV $< M_{\mathrm{T}} <$ 80 GeV. The numbers of events expected and measured in this control region can be found in Table 3. The normalization factor for the control region was calculated to be 2.1 ± 1.0. The uncertainty in the normalization factor is large because of the small number of events in the control region but the factor is consistent with one. A systematic uncertainty was assigned in addition to the extrapolation of this number from the control region to the full phase space. The total conservative uncertainty assigned to this prediction is 50%.

8 Systematic uncertainties

To estimate the Standard Model prediction several of the most important sources of experimental systematic uncertainties on the Monte Carlo predictions have been considered. Firstly the uncertainty associated with the measurement of the calorimeter energy scale was estimated using a parameterization of the energy scale as a function of jet p_{T} and η [29]. This procedure was designed to produce a conservative estimate of the uncertainty. Jets have a fractional uncertainty of typically 10% if the jet transverse momentum is in the range $20 < p_{\mathrm{T}} < 60$ GeV and 7% for jets at higher p_{T}. The effect of the change in energy scale was applied in a fully correlated way to jets in all Monte Carlo samples and to the component of the missing transverse momentum from clusters associated with those jets.

The lepton fake rate was studied by reversing the lepton isolation criteria with good agreement between the data and the QCD Monte Carlo simulation being found. The QCD background procedure was also compared with the `ALPGEN` QCD sample and again satisfactory agreement was found. From those studies a conservative systematic uncertainty of 50% is assigned to the overall normalization of the QCD prediction to the one-lepton channels. The uncertainty for the 2-lepton channels is 100%. We have attributed a 60% normalization uncertainty for Z + jets production.

The uncertainty in the integrated luminosity is estimated to result in an overall normalization error of 11% for $t\bar{t}$ production.

Uncertainties associated with the trigger efficiency, and electron and muon identification efficiency are small by comparison.

The statistical uncertainty (assumed to be $\sqrt{N}$) on the Monte Carlo prediction and all systematic uncertainties are added in quadrature. No attempt has been made in this early study to distingusish between errors correlated and uncorrelated between bins or selections.

9 Results

Selections and distributions are made for the following variables.

Missing transverse momentum The calorimeter transverse missing energy components are defined by

$$\begin{aligned} E_x^{\text{miss,calo}} &\equiv -\sum_{i=1}^{N_{\text{cell}}} E_i \sin\theta_i \cos\phi_i \\ E_y^{\text{miss,calo}} &\equiv -\sum_{i=1}^{N_{\text{cell}}} E_i \sin\theta_i \sin\phi_i \end{aligned}$$

where the sum is over topological cluster cell energies at the electromagnetic scale within the pseudo-rapidity range $|\eta| < 4.5$. In the following definitions the missing transverse momentum two-vector is corrected by subtracting the transverse momentum from any isolated muons,

$$\vec{E}_{\text{T}}^{\text{miss}} \equiv (E_x^{\text{miss,calo}}, E_y^{\text{miss,calo}}) - \sum_j \mathbf{p}_{\text{T}}^{\mu,j}. \quad (1)$$

The missing transverse momentum $E_{\text{T}}^{\text{miss}}$ is defined as the norm of the $\vec{E}_{\text{T}}^{\text{miss}}$ vector.

The performance of the missing transverse momentum reconstruction during the data-taking period is described in Ref. [30]. Events in which invisible particles are produced can be expected to have large $E_{\text{T}}^{\text{miss}}$.

Effective mass (M_{eff}) is the scalar sum of transverse momenta of all main objects and is defined as the sum

$$M_{\text{eff}} \equiv \sum_{i=1}^{N_{\text{jets}}} p_{\text{T}}^{\text{jet},i} + \sum_{j=1}^{N_{\text{lep}}} p_{\text{T}}^{\text{lep},j} + E_{\text{T}}^{\text{miss}}$$

where N_{jets} is the minimum number of jets required for the analysis channel, which is two in this paper, and N_{lep} is the number of leptons required (one or two depending on the channel). If more than two jets pass the selection, the two with the largest p_{T} are used in the sum. Other high p_{T} jets or leptons are not included in the sum.

The data are shown for all distributions as points, with Poisson interval error bars to allow the reader to estimate the statistical uncertainty. All results are compared to the Monte Carlo expectation for QCD, $W^{\pm}$ + jets, Z^0 + jets and $t\bar{t}$ production.

After requiring a single lepton with $p_{\text{T}} > 20$ GeV, two jets with $p_{\text{T}} > 30$ GeV and $E_{\text{T}}^{\text{miss}} > 30$ GeV the selection efficiency times branching ratios for the SU4 SUSY model point used for comparison was 6.1% for the single electron mode and 5.4% for the single muon mode.

9.1 Distributions for the one-lepton analysis

Figure 1 shows the missing transverse momentum distribution for events in the electron channel (before any $E_{\mathrm{T}}^{\mathrm{miss}}$ or m_{T} cut is applied). The data are in agreement with the Monte Carlo prediction which is dominated by the QCD background up to $E_{\mathrm{T}}^{\mathrm{miss}}$ of about 40 GeV. For higher values of $E_{\mathrm{T}}^{\mathrm{miss}}$ the dominant contribution is from $W^{\pm}$ + jets. The SUSY model would tend to yield higher values of missing transverse momentum as can be seen in Fig. 1. Two events are found after a cut on the transverse mass $m_{\mathrm{T}} > 100$ GeV, consistent with the expectation from Standard Model processes. Such a cut would enhance the signal-to-background ratio for typical SUSY models with an mSUGRA-like mass spectrum.

Figure 2 shows the corresponding results for the muons channel. The simulations provide a reasonably good description of the data. The properties of the events with $E_{\mathrm{T}}^{\mathrm{miss}} > 30$ GeV have been individually checked. One event is found after a cut on the transverse mass $m_{\mathrm{T}} > 100$ GeV, again consistent with the expectation from Standard Model processes. For each, the muons were reconstructed with each of two independent tracking algorithms. There is no evidence of noise in the calorimeter, nor nearby jets. In each case the muon was found to be well-isolated (both in terms of lack of nearby calorimeter energy and absence of nearby tracks), has a good track fit matching in the inner detector and the data, with a well-matched relative p_{T}. The timing of the hits on these tracks has been checked using precision timing available from the monitored drift tubes and the transition radiation tracker. In each case the timing of the hits is as expected from a track from the interaction point (to within the resolution of order 2 ns). Such a good timing match would not be expected for tracks originating from cosmic rays for which one would expect the timing to be only approximately coincident with the primary collision. All of the jets have well-matched tracks and none show any of the features which might identify them as noise hits.

The distributions of the effective mass are shown in Figs. 3 and 4 for the electron and muon channel, respectively. The Standard Model predictions are dominated by the QCD background for all effective mass values when no cut on $E_{\mathrm{T}}^{\mathrm{miss}}$ is applied. The data are generally in good agreement with the predictions. One event in the muon channel has a particularly large value of M_{eff}, above 900 GeV. A graphical display of this event can be found in the appendix.

After a cut requiring $E_{\mathrm{T}}^{\mathrm{miss}} > 30$ GeV the $W^{\pm}$ + jets sample is the dominant Standard Model process. Figure 5 shows the distribution of the transverse mass before the cut on $E_{\mathrm{T}}^{\mathrm{miss}}$ for the electron and muon channels. The QCD background dominates in the electron channel. In the muon channel the QCD background dominates only at low values of m_{T} and $W^{\pm}$ + jets production gives the largest contribution at high values. At high m_{T} the muon distribution contains many of the same events that could be observed at high $E_{\mathrm{T}}^{\mathrm{miss}}$ in Fig. 2 (a) and large M_{eff} in Figs. 4 (a) and (b).

Figure 6 shows the same variable with a cut on $E_{\mathrm{T}}^{\mathrm{miss}}$. After this cut is applied $W^{\pm}$ + jets production dominates for both channels. The data are consistent with the expectation from the $W^{\pm}$ + jets Monte Carlo. The events identified previously at high $E_{\mathrm{T}}^{\mathrm{miss}}$ are also observed in Fig. 6 (b).

The jet multiplicity distributions for the electron and muon channels can be found in Fig. 7. The number of events after several stages of the selection can be found in Table 4.

9.2 Distributions for the two lepton analysis

The two-lepton analysis selection requires two leptons with $p_{\mathrm{T}} > 10$ GeV, one of which must have $p_{\mathrm{T}} > 20$ GeV. The dilepton invariant mass is required to be greater than 5 GeV. Figure 8 shows the missing transverse momentum distribution for events passing this selection subdivided in lepton pairs of opposite sign and lepton pairs of same sign. Two events are found in the opposite sign channel with $E_{\mathrm{T}}^{\mathrm{miss}} > 30$ GeV, consistent with the expectation of 2.0 ± 0.8 from Standard Model processes.

Selection	Electron channel		Muon channel	
	Data	Monte Carlo	Data	Monte Carlo
$p_{\mathrm{T}}(\ell) > 20$ GeV $\cap$ ≥ 2 jets with $p_{\mathrm{T}} > 30$ GeV	143	157 ± 85	40	37 ± 14
$\cap\, E_{\mathrm{T}}^{\mathrm{miss}} > 30$ GeV	13	16 ± 7	17	15 ± 7
$\cap\, m_{\mathrm{T}} > 100$ GeV	2	3.6 ± 1.6	1	2.8 ± 1.2

Table 4: Number of events observed and predicted at several stages of the single lepton selection. As described in Section 7, the Monte Carlo predictions have been normalised to the data in control regions which overlap all but the final selection.

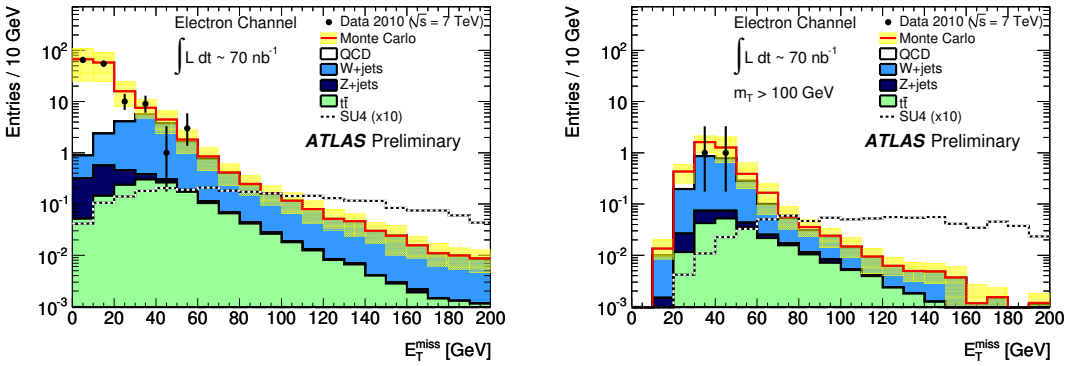

(a) (b)

Figure 1: Distributions of the missing transverse momentum for events in the electron channel, without (a) and with (b) a cut on the transverse mass $m_{\mathrm{T}} > 100$ GeV. No requirement on $E_{\mathrm{T}}^{\mathrm{miss}}$ has been applied.

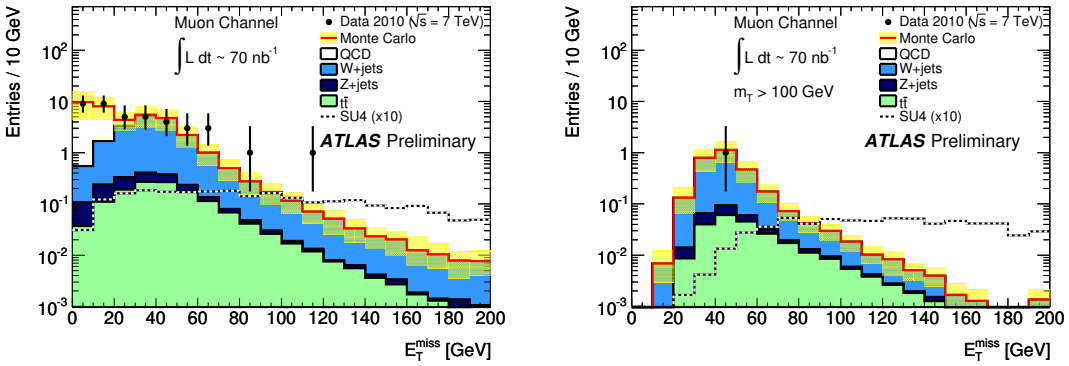

(a) (b)

Figure 2: Distributions of the missing transverse momentum for events in the muon channel, without (a) and with (b) a cut on the transverse mass $m_{\mathrm{T}} > 100$ GeV. No requirement on $E_{\mathrm{T}}^{\mathrm{miss}}$ has been applied.

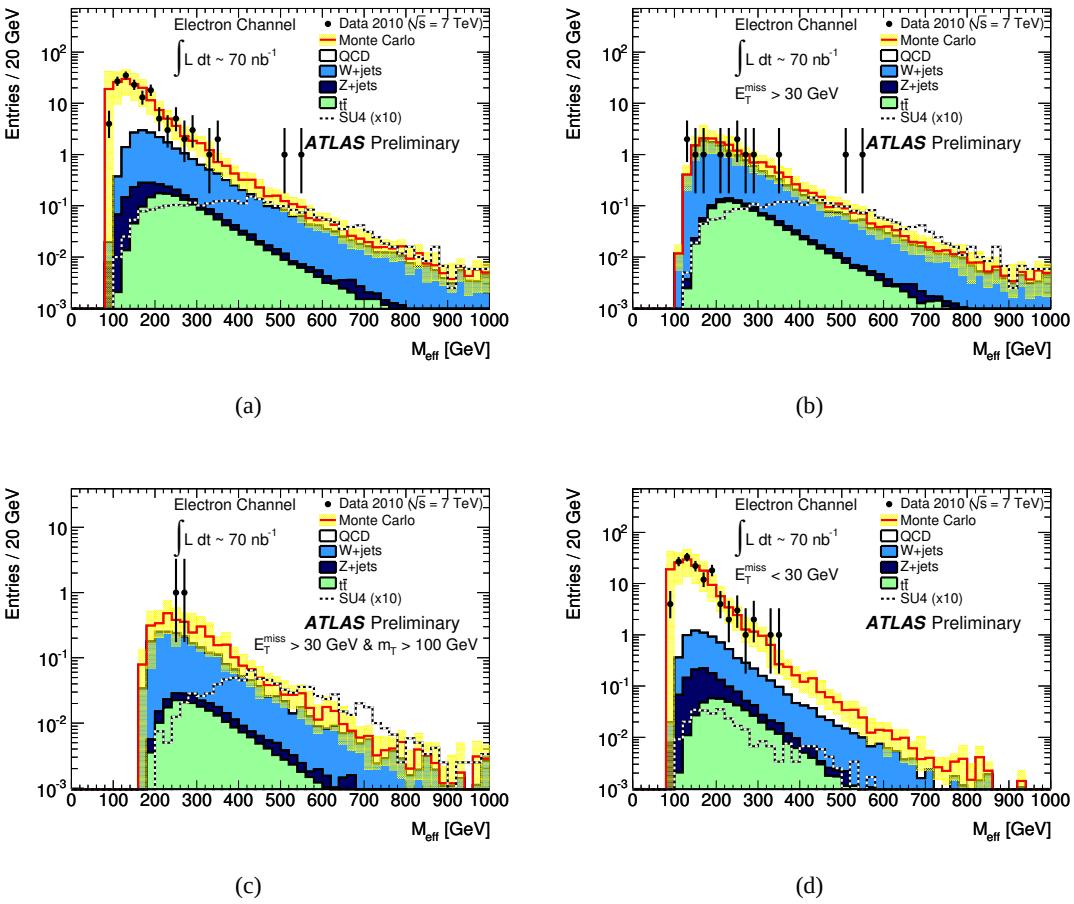

Figure 3: Distribution of the effective mass for events in the electron channel. No cut on $E_{\mathrm{T}}^{\mathrm{miss}}$ has been applied in (a). A cut requiring $E_{\mathrm{T}}^{\mathrm{miss}} > 30$ GeV is applied in (b). In (c) both $E_{\mathrm{T}}^{\mathrm{miss}} > 30$ GeV and $m_{\mathrm{T}} > 100$ GeV are required. In (d) the missing transverse momentum cut is reversed so that $E_{\mathrm{T}}^{\mathrm{miss}} < 30$ GeV.

10 Summary and conclusion

An analysis of the first $70 \pm 8\,\mathrm{nb}^{-1}$ of integrated luminosity collected with the ATLAS detector is presented. These data are analysed in an early search for new physics in channels containing jets, and missing transverse momentum together with one or more leptons (electrons or muons). The measurements are compared to simulations based on Monte Carlo predictions of Standard Model QCD, gauge boson + jets and $t\bar{t}$ processes using the ATLAS GEANT-based full detector simulation.

The measured distributions of jet momenta, missing transverse momentum, effective mass, and transverse mass generally show agreement with expectations from Standard Model processes.

One of the single-muon events contains five jets with $p_{\mathrm{T}} > 30$ GeV and an unusually large scalar sum of transverse momentum (greater than 1.2 TeV). A graphical display of this event can be found in the appendix.

After a further cut requiring $m_{\mathrm{T}} > 100$ GeV two events remain in the single electron channel and one event is found in the single muon channel. The Standard Model expectation after this further selection is 3.6 ± 1.6 events in the electron channel and 2.8 ± 1.2 events in the muon channel.

When requiring a second lepton (e or μ) with $p_{\mathrm{T}} > 10$ GeV and $E_{\mathrm{T}}^{\mathrm{miss}} > 30$ GeV, two events remain in

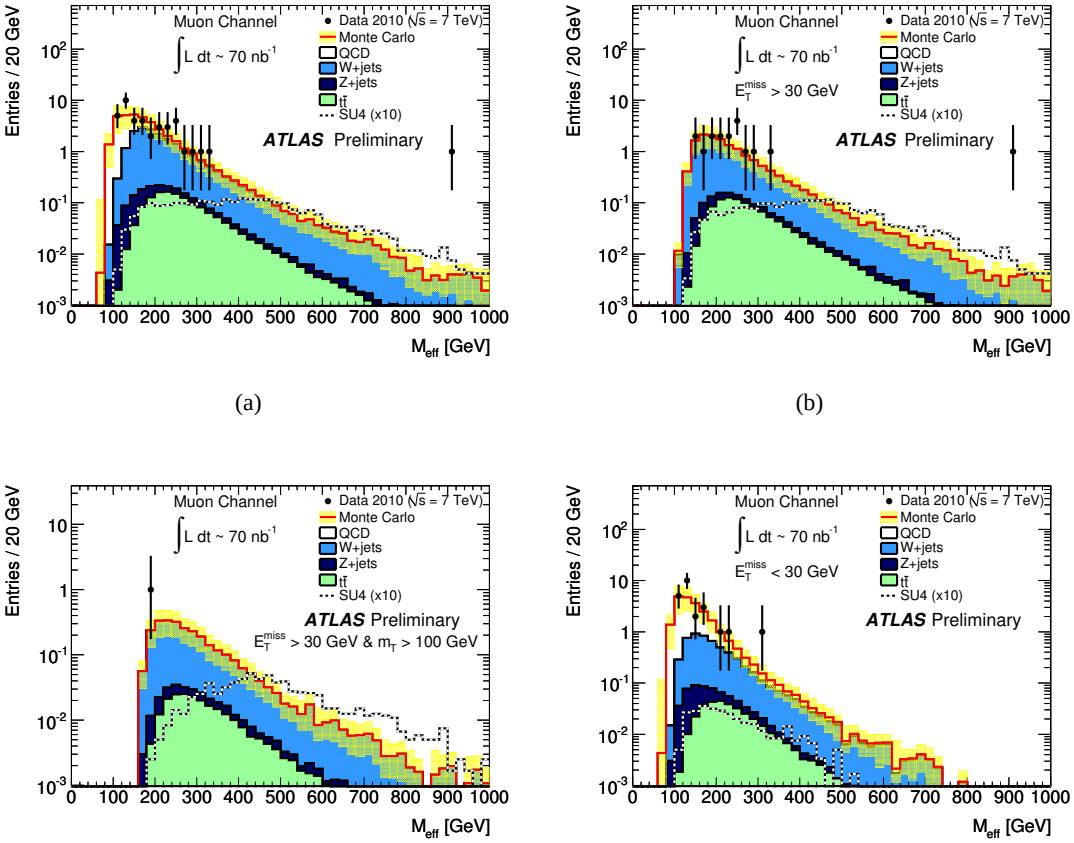

Figure 4: Distribution of the effective mass for events in the muon channel. In (a) no cut on $E_{\mathrm{T}}^{\mathrm{miss}}$ is applied. In (b) a cut requiring $E_{\mathrm{T}}^{\mathrm{miss}} > 30$ GeV is applied. In (c) both $E_{\mathrm{T}}^{\mathrm{miss}} > 30$ GeV and $m_{\mathrm{T}} > 100$ GeV are required. In (d) the missing transverse momentum cut is reversed so that $E_{\mathrm{T}}^{\mathrm{miss}} < 30$ GeV.

the data in the opposite sign channel, consistent with the expectation of 2.0 ± 0.8 from Standard Model processes.

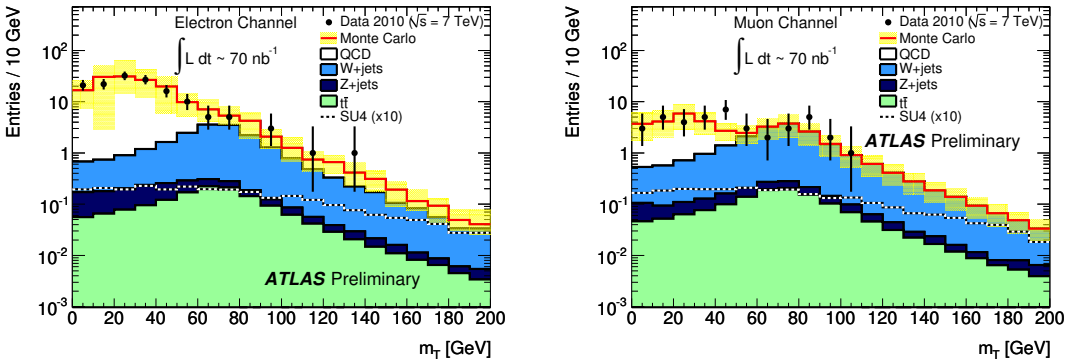

(a) (b)

Figure 5: Distributions of the transverse mass m_{T} without a cut on $E_{\mathrm{T}}^{\mathrm{miss}}$ for the electron (a) and muon channel (b).

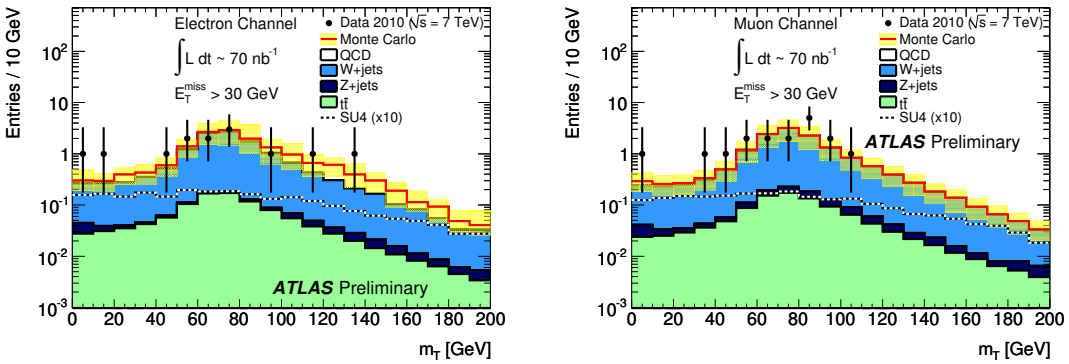

(a) (b)

Figure 6: Distributions of the transverse mass m_{T} with a cut on $E_{\mathrm{T}}^{\mathrm{miss}} > 30$ GeV for the electron (a) and muon channel (b).

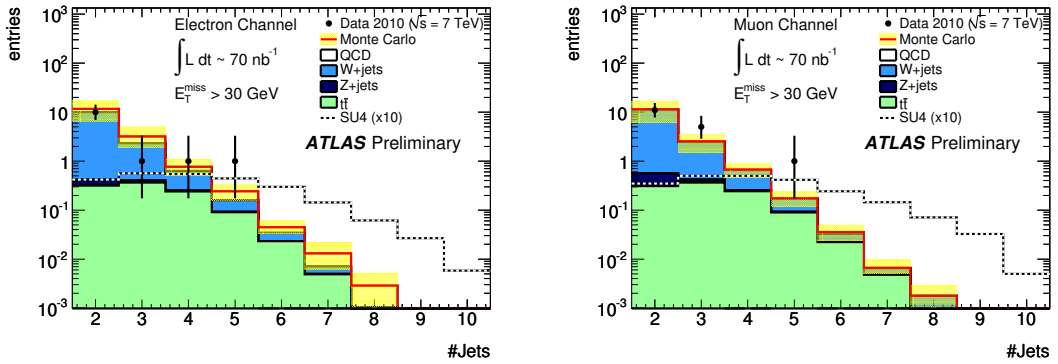

(a) (b)

Figure 7: Distribution of the number of jets with $p_{\mathrm{T}} > 30$ GeV for the electron (a) and muon channel (b). The cut requiring $E_{\mathrm{T}}^{\mathrm{miss}} > 30$ GeV has been applied.

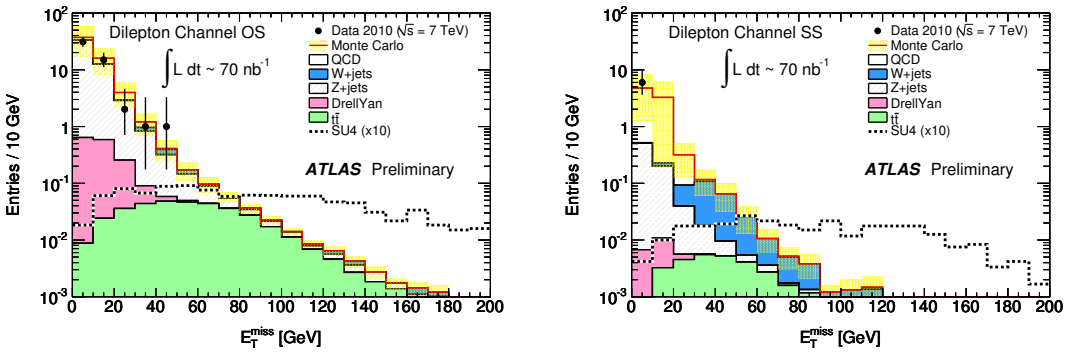

(a) (b)

Figure 8: Distribution of the missing transverse momentum for di-lepton events. The cuts applied are described in the text.

References

[1] Y.A. Golfand and E.P. Likhtman, JETP Lett. **13** (1971) 323–326; A. Neveu and J.H. Schwarz, Nucl. Phys. **B31** (1971) 86–112; A. Neveu and J.H. Schwarz, Phys. Rev. **D4** (1971) 1109–1111; R. Ramond, Phys. Rev. **D3** (1971) 2415–2418; D.V. Volkov and V.P. Akulov, Phys. Lett. **B46** (1973) 109–110; J. Wess and B. Zumino, Phys. Lett. **B49** (1974) 52; J. Wess and B. Zumino, Nucl. Phys. **B70** (1974) 39–50.

[2] L. Evans and P. Bryant, JINST **3** (2008) S08001.

[3] The ATLAS collaboration, JINST **3** (2008) S08003.

[4] The ATLAS collaboration, Observation of $W \to \ell\nu$ and $Z \to \ell\ell$ production in proton-proton collisions at $\sqrt{s} = 7\,\text{TeV}$ with the ATLAS detector, ATLAS-CONF-2010-044, June 2010.

[5] The ATLAS collaboration, Observation of energetic jets in pp collisions at $\sqrt{s} = 7\,\text{TeV}$ using the ATLAS experiment at the LHC, ATLAS-CONF-2010-043, June 2010.

[6] The ATLAS collaboration, Prospects for supersymmetry discovery based on inclusive searches at a 7 TeV centre-of-mass energy with the ATLAS detector, ATL-PHYS-PUB-2010-010, June 2010.

[7] T. Aaltonen *et al.*, Phys. Rev. Lett. **102** (2009) 121801; Abazov, V. M. *et al.*, Phys. Lett. **B660** (2008) 449–457.

[8] T. Sjostrand, and S. Mrenna and P. Skands, JHEP **05** (2006) 026.

[9] G. Corcella *et al.*, JHEP **01** (2001) 010; G. Corcella *et al.*, *HERWIG 6.5 release note*, hep-ph/0210213, 2002.

[10] J. Butterworth, J. Forshaw and M. Seymour, Z. Phys. **C72** (1996) 637–646.

[11] The ATLAS collaboration, ATLAS Monte Carlo tunes for MC09, ATL-PHYS-PUB-2010-002, 2010.

[12] S. Agostinelli *et al.*, Nucl. Instrum. Meth. **A506** (2003) 250–303.

[13] A. Sherstnev and R.S. Thorne, Eur. Phys. J. **C55** (2008) 553–575.

[14] M. Mangano *et al.*, JHEP **07** (2003) 001.

[15] D. Stump *et al.*, JHEP **10** (2003) 046.

[16] C. Anastasiou, L.J. Dixon, K. Melnikov, and F. Petriello, Phys. Rev. **D69** (2004) 094008.

[17] S. Frixione and B.R. Webber, The MC@NLO 3.2 event generator, hep-ph/0601192, 2006.

[18] S. Frixione and B.R. Webber, JHEP **06** (2002) 029.

[19] S. Moch and P. Uwer, Nucl. Phys. Proc. Suppl. **183** (2008) 75–80.

[20] R. Barbieri and S. Ferrara and C.A. Savoy, Physics Letters B **119** (1982) 343 – 347; L.J. Hall and J.D. Lykken, and S. Weinberg, Phys. Rev. D **27** (1983) 2359–2378.

[21] F.E. Paige, S.D. Protopopescu, H. Baer, and X. Tata, ISAJET 7.69: A Monte Carlo event generator for p p, anti-p p, and e+ e- reactions, hep-ph/0312045, 2003.

[22] M. Bahr *et al.*, Eur. Phys. J. **C58** (2008) 639–707; M. Bahr *et al.*, Herwig++ 2.3 release note, arXiv:0812.0529, 2008.

[23] W. Beenakker, R. Hopker and M. Spira, PROSPINO: A program for the production of supersymmetric particles In next-to-leading order QCD, hep-ph/9611232, 1996.

[24] The ATLAS collaboration, Expected performance of the ATLAS experiment – detector, trigger and physics, page 1589-1616, arXiv:0901.0512, 2009.

[25] M. Cacciari, G.P. Salam and G. Soyez, JHEP **04** (2008) 063.

[26] The ATLAS collaboration, Data-quality requirements and event cleaning for jets and missing transverse energy reconstruction with the ATLAS detector in proton-proton collisions at a center-of-mass energy of $\sqrt{s} = 7$ TeV, ATLAS-CONF-2010-038.

[27] The ATLAS collaboration, Early supersymmetry searches in channels with jets and missing transverse momentum with the ATLAS detector, ATLAS-CONF-2010-065, July 2010.

[28] V.M. Abazov *et al.*, Phys. Lett. **B669** (2008) 278–286.

[29] The ATLAS collaboration, Jet energy scale and its systematic uncertainty in ATLAS for jets produced in proton-proton collisions at $\sqrt{s} = 7$ TeV, ATLAS-CONF-2010-056, June 2010.

[30] The ATLAS collaboration, Performance of the missing transverse energy reconstruction in minimum bias collisions at center-of-mass energy of $\sqrt{s}$ = 7 TeV with the ATLAS detector, ATLAS-CONF-2010-057, 2010.

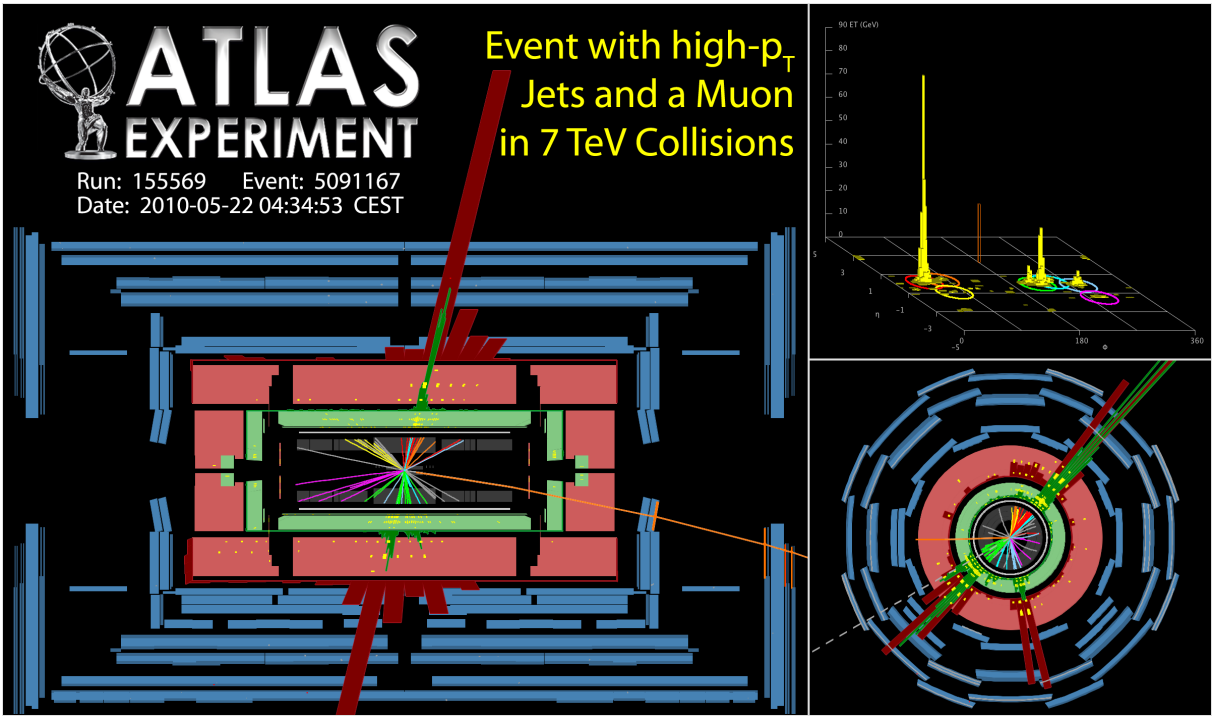

Figure 9: Event display of the collision (run number 155569, event number 5091167) with M_{eff} of 915 GeV when only the leading two jets are included in the scalar sum increasing to 1156 GeV if all jets are included. There are a total of 145 tracks associated with the primary vertex; no second vertex is reconstructed. The missing transverse momentum is 118 GeV. There is one well isolated positively charged muon with p_{T} of 25 GeV, and $\eta = 2.33$. That muon is cleanly selected with 11 hits on the monitored drift tubes, 6 on the cathode strip chambers, 5 pixel hits and 8 silicon strip hits.